

Intraslab seismicity and thermal stress in the subducted Cocos plate beneath central Mexico

Vlad Manea*, Marina Manea, Vladimir Kostoglodov, Granville Sewell

GPS Caltech Seismological Laboratory, 1200E California Boulevard MS 252-21, Pasadena, CA 91125, United States

Received 20 June 2004; received in revised form 29 December 2005; accepted 22 March 2006

Abstract

We present a model of the subducting Cocos slab beneath Central Mexico, that provides an explanation for stresses causing the occurrence of the majority of the intraslab earthquakes which are concentrated in a long flat segment. Based on the recently developed thermal models for the Central Mexico subduction zone, the thermal stresses due to non-uniform temperature contrast in the subducting slab are calculated using a finite element approach. The slab is considered purely elastic but due to high temperature at its bottom the behavior is considered as ductile creep. The calculation results show a ~ 20 km slab core characterized by a tensional state of stress with stresses up to 70 MPa. On the other hand, the top of the slab experiences high compressive thermal stresses up to 110 MPa, depending on the elastic constants used and location along the flat part of the subducting plate. These compressive stresses at the top of the slab are not consistent with the exclusive normal fault intraslab earthquakes, and two different sources of stress are proposed.

The trenchward migration of the Mexican volcanic arc for the last 7 Ma indicates an increase of the slab dip through time. This observation suggests that the gravity torque might exceed the suction torque. Considering the flat slab as an embedded plate subject to an applied clockwise net torque of 0.5×10^{16} – 1.5×10^{16} N m, the upper half would exhibit tensional stresses of 40–110 MPa that can actually balance the compressive thermally induced stresses.

An alternative stress source might come from the slab pull force caused by the slab positive density anomaly. Based on our density anomaly estimations (75 ± 20 kg/m³), a 350 km slab length, dipping at 20° into the asthenosphere, induces a slab pull force of 1.7×10^{12} – 4.6×10^{12} N m. This force produces a tensional stress of 41–114 MPa, sufficient to balance the compressive thermal stresses at the top of the flat slab.

The linear superposition of the thermally and torque or slab pull induced stresses shows tensile stresses up to 60–180 MPa inside the flat slab core. Also, our results suggest that the majority of the intraslab earthquakes inside the flat slab are situated where the resultant stresses are larger than 40–80 MPa.

This study provides a reasonable explanation for the existence of exclusively normal fault intraslab earthquakes in the flat slab beneath Central Mexico, and also it shows that thermal stresses due to non-uniform reheating of subducting slabs play a considerable role in the total stress field.

© 2006 Elsevier B.V. All rights reserved.

Keywords: Thermal stress; Torque balance; Slab pull; Flat subduction; Mexican subduction zone

* Corresponding author.

1. Introduction

It has been proposed that the cold subducted oceanic lithosphere, entering into the hotter mantle, produces significant thermal stresses that might generate intraslab earthquakes. Thermal stress distribution has been proposed as possible explanations for a double fault plane in various subduction zones such as Japan and Kamchatka (Hamaguchi et al., 1983; Gorbatov et al., 1997). Thermal stress has been proposed as a main contributor to the formation of transform faults (Turcotte, 1974; Collette, 1974). Bratt et al. (1985) show that thermoelastic stresses are an important cause for earthquakes in young oceanic lithosphere. Zhu and Wiens (1991) demonstrate that thermal stress due to reheating of oceanic lithosphere is an important contributor to the stress field in the oceanic lithosphere near hotspots. Despite their importance, only a few studies of thermal stresses in the subducting slabs have been published (Hamaguchi et al., 1983; Goto et al., 1985). The main problem in these studies is the magnitude of the thermally induced stresses which can exceed 1 GPa. These excessive values of the thermal stresses are probably related to temperature contrasts as

high as 1000 °C in the subducting slab, assuming a 0 °C initial slab temperature. Although the state of stress in the subducting slabs represents the input from many sources, thermal stresses can contribute significantly to the state of intraplate stress in the oceanic lithosphere (Haxby and Parmentier, 1988), especially where a long flat segment of the slab exists. This might be the case for Central Mexico where a long flat segment of the subducted Cocos slab, extending from ~ 100 km up to ~ 270 km from the trench, comprises ~ 90% of the normal-fault intraslab earthquakes (Fig. 1).

Bending stresses due to concave/convex shape of the subducting slab are very difficult to determine (Goto et al., 1985) because they are very sensitive to the curvature of the plate that has large uncertainties in Mexico. Slab pull of the denser subducting slab and the associated down flexure of the slab produce important deviatoric tension of up to several hundreds MPa. Also, important stress concentrations and pressure variations (up to some hundreds MPa) due to the shape of the subducting slab along the thrust fault, might significantly contribute to the state of stress (Manea et al., 2004). In addition, the stress in the slab depends on whether the thrust fault is locked or unlocked, producing variations of the slab

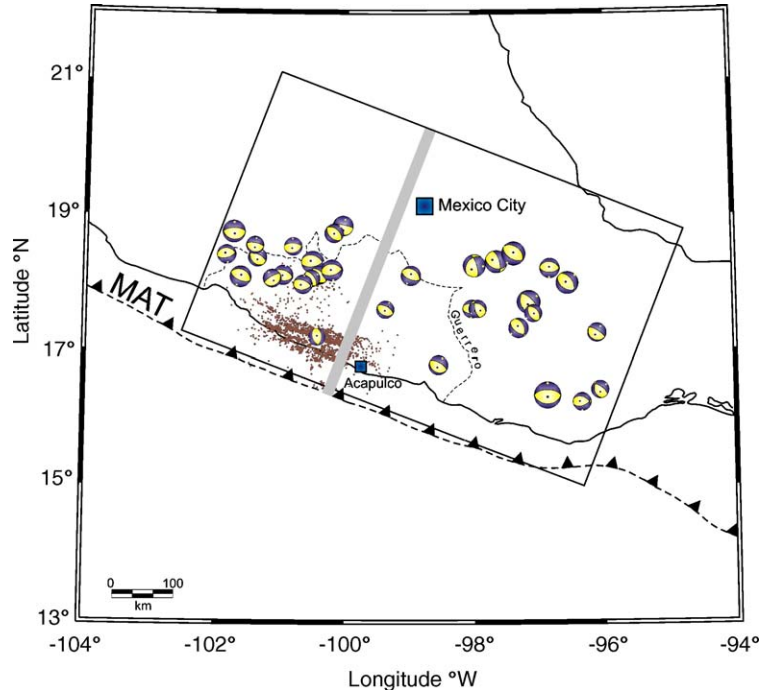


Fig. 1. The position of the modeled cross-section in Guerrero, Central Mexico. Brown dots represent the epicenters of the events registered by the regional seismic network of IGF UNAM in Guerrero (1987–1992) (Kostoglodov et al., 1996). Thick gray line represents the 2D model cross-section. MAT — Middle America Trench. Focal mechanisms represent the intraslab normal fault events with magnitude greater than 5.0 (M_w) (compilation from: Jiménez and Ponce, 1978; Singh et al., 1985; González-Ruiz, 1986; Lefevre and McNally, 1985; Pardo and Suárez, 1995; Singh and Pardo, 1993; Lay et al., 1989; Dean and Drake, 1978; Engdahl and Villaseñor, 2002; Gonzalez-Ruiz and McNally, 1988; CMT, Harvard catalog; Iglesias et al., 2002).

interior stress. Another source of stress comes from the ridge push. This might be an order of magnitude smaller than the trench pull (Turcotte and Schubert, 2002), but the resistive forces encountered by the descending oceanic lithosphere into the mantle may compensate this difference. The olivine–spinel phase change inside the slab (~ 400 km depth), might give rise to important tensional and compressive stresses up to 1 GPa (Goto et al., 1985). During subduction, the hydrated basalts and gabbros are transformed into the higher density eclogite and this may induce deviatoric stresses. In warm subduction zones dehydration due to the basalt–eclogite transformation and intraslab earthquakes occur at shallower depths (Kirby, 2000).

A space-time evolution of the Mexican volcanic arc, shows that in the last 7 Ma the volcanic arc migrated toward the trench with ~ 70 km (Ferrari et al., 1999). The changing in the position of the volcanic arc through time reflects the increasing of the slab dip (Poli and Schmidt, 2002). The gravity force exerts a torque on the descending slab, which bends the slab vertically. On the other hand, the suction force tends to lift up the slab (Jischke, 1975; Tovish et al., 1978). The competition between these two major forces sets the slab dip evolution in time.

Recent improvements in numerical methods allow the development of high-resolution thermo-mechanical models of subducting slabs with temperature and/or stress dependent rheology (Furukawa, 1993; Conder et

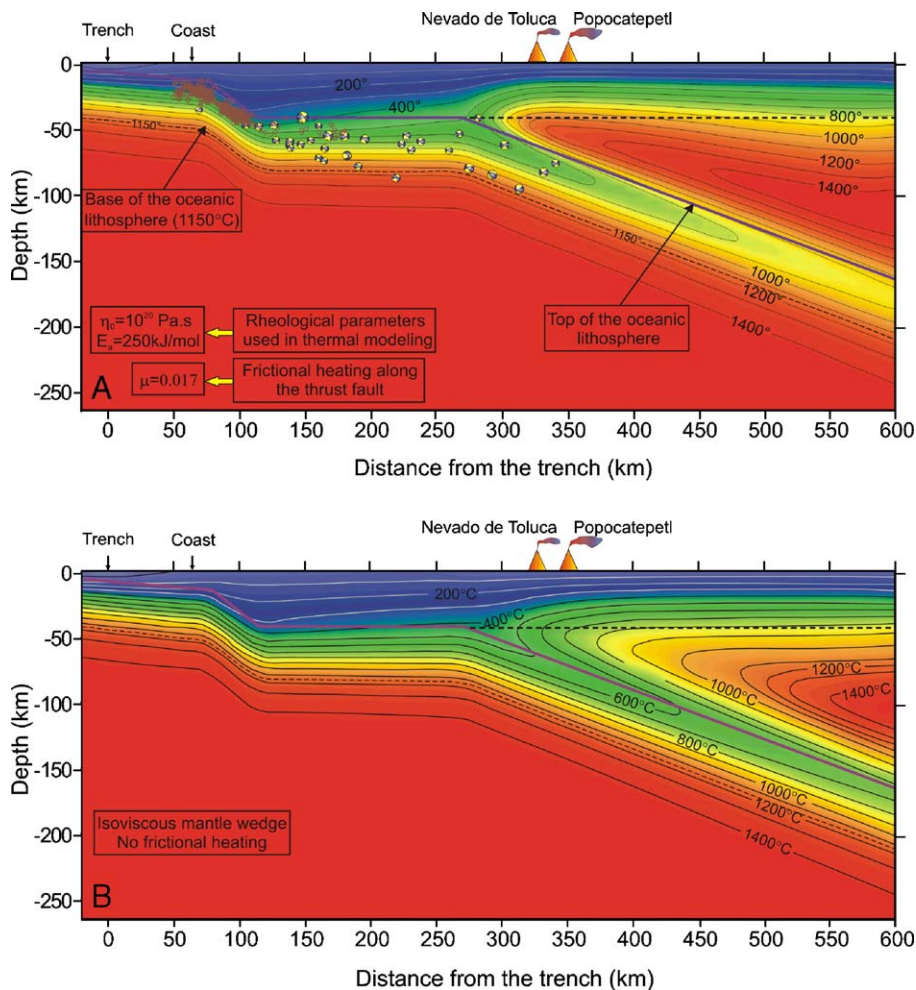
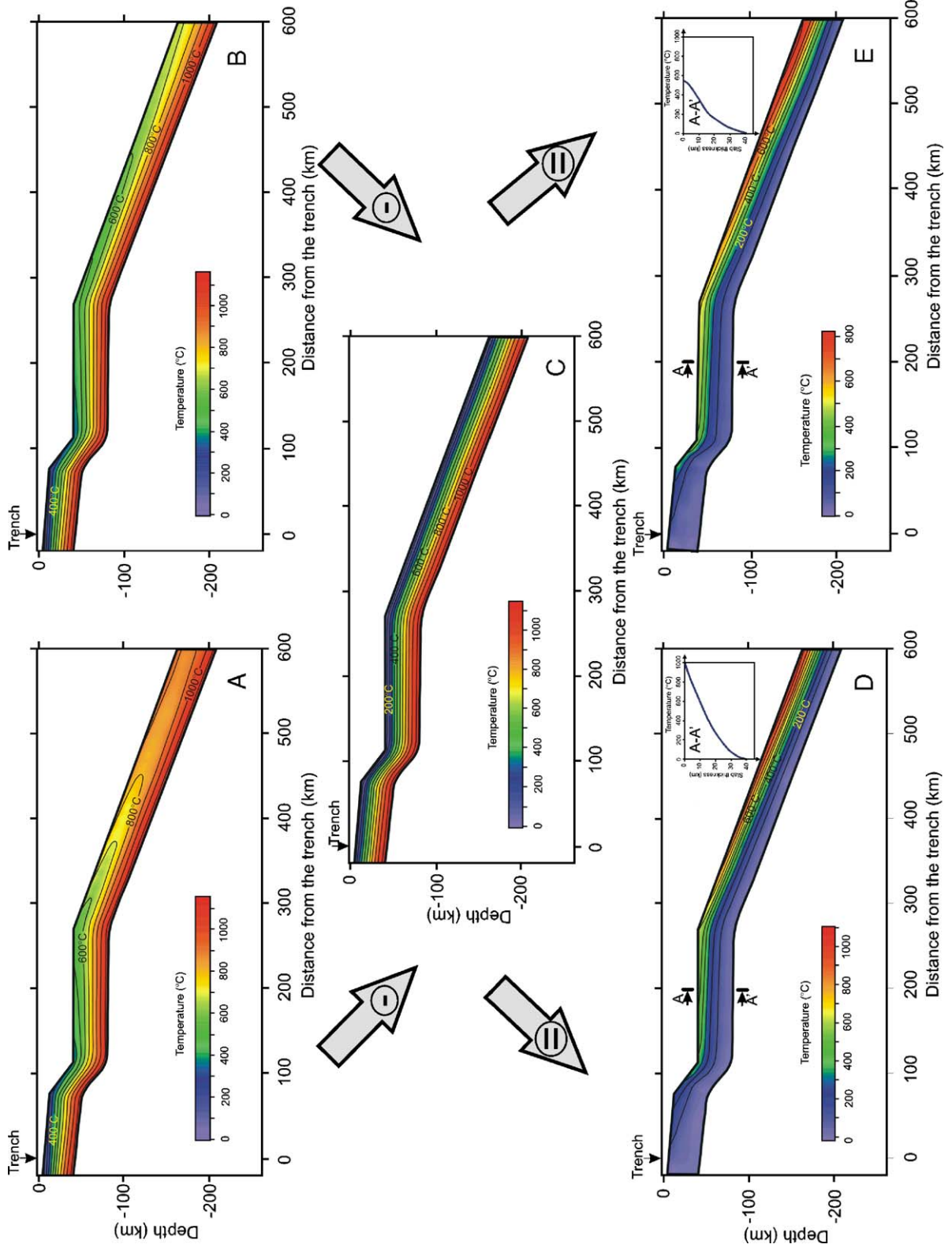


Fig. 2. Thermal models for Central Mexico from Manea et al. (2005). The focal mechanisms represent the intraplate seismicity with magnitude greater than 5.0 (M_w) from Fig. 1. Brown clouds of hypocenters (Kostoglodov et al., 1996) beneath the coast denote the smaller magnitude seismicity associated probably with the bending–unbending of the subducted slab beneath the coast. Thick violet solid line denotes the top of the subducting slab. Horizontal black dashed line shows the Moho (40 km depth). Dashed black line represents the base of the oceanic lithosphere. A. Steady-state thermal models with strong temperature dependent viscosity in the mantle wedge for activation energy $E_a = 250$ kJ/mol and reference viscosity, $\eta_0 = 10^{20}$ Pa s. Frictional heating along the thrust fault is considered; B. Calculated steady state thermal field for the isoviscous mantle wedge with no frictional heating along the thrust fault. (For interpretation of the references to colour in this figure legend, the reader is referred to the web version of this article)



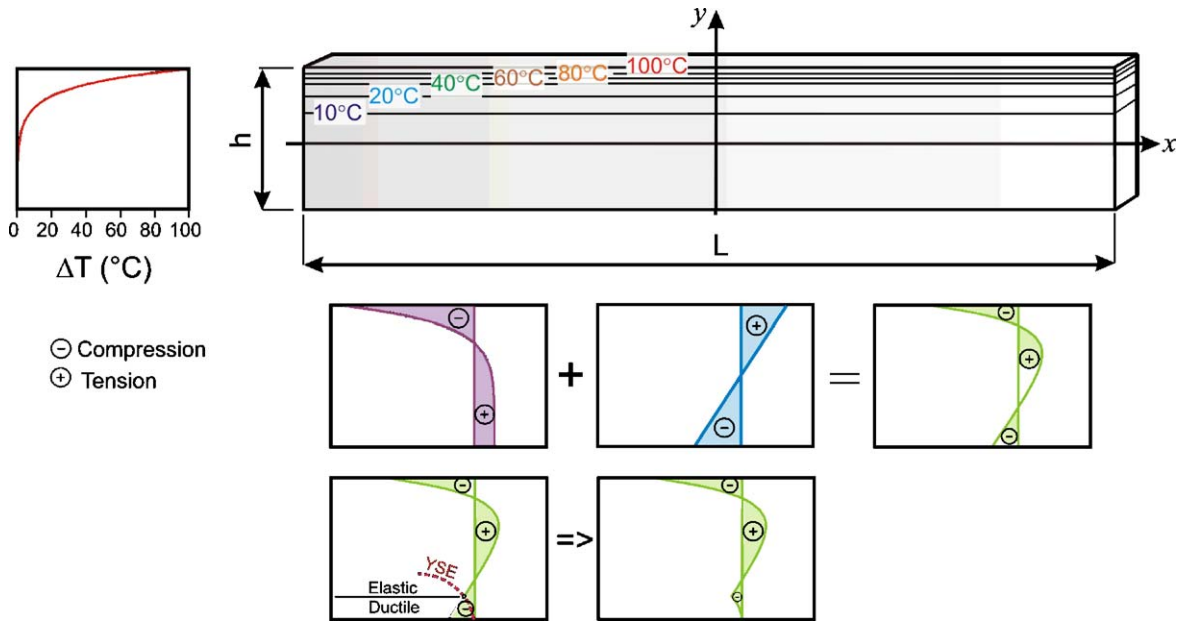


Fig. 4. Simple example showing thermal stresses in an elastic and unconstrained slab due to an exponential heating. Thermal stresses can actually be separated into two parts: thermo-dilatation and thermo-bending stresses.

al., 2002; van Keken et al., 2002; van Hunen et al., 2003; Kelemen et al., 2003; Manea et al., 2005). In this study, thermal stresses induced in the subducted slab due to non-uniform temperature distribution (Manea et al., 2004, 2005) are inferred using a finite element technique. Also, we investigate the effect of the net torque balance (gravity torque–suction torque), and slab pull, on the flat slab. It is shown that the thermal stresses are approximately one order of magnitude smaller than the previous published results. In addition, this study offers a feasible explanation for the occurrence of exclusively normal fault intraslab earthquakes in the flat slab beneath Central Mexico, using the superposition of thermal stresses and stresses induced by the suction and gravity torque balance or by the slab pull forces.

2. Model formulation

2.1. Thermal models

The main input parameter in this study is the 2D steady state thermal model from Manea et al., 2005 (Fig.

2). Using the finite element solver PDE2D (<http://pde2d.com/>) the thermal model is obtained by solving numerically the Stokes equations for the mantle wedge and heat transfer equation for the entire model. This model incorporates a strong temperature-dependent viscosity formulation which makes the system of equations strongly nonlinear and a cut-off viscosity of 10^{24} Pa s for the temperature less than 1100°C was used to achieve a convergent solution. Since most of the subducting slab is colder than 1100°C , it has a viscosity $\sim 10^{24}$ Pa s. An uneven mesh (higher resolution in the tip of the mantle wedge) with 12,000 triangular shaped elements was used. The slab was considered as a rigid body with a prescribed velocity of 5.5 cm/yr (DeMets et al., 1994). A test with reasonably varied parameters (slab age 14 ± 1 Ma, thermal conductivities varied with $\pm 10\%$, coefficient of friction $0\text{--}0.017$) shows uncertainties in the thermal model of $\pm 50^\circ\text{C}$ to $\pm 100^\circ\text{C}$. Fig. 2A presents a steady-state thermal model with strong temperature dependent viscosity in the mantle wedge, which shows a hotter mantle wedge and slab beneath the volcanic arc than the model with an isoviscous mantle (Fig. 2B). Also, one of

Fig. 3. The temperature variation ΔT that actually causes thermal stresses represents the difference between the actual slab temperature and a reference slab temperature for which the slab is considered stress free. A. “Hot” thermal model from Fig. 2A shown here only inside the subducting slab; B. “Cold” thermal model from Fig. 2B shown here only inside the subducting slab; C. Reference thermal model corresponding to a 14 Ma oceanic plate geotherm; D. Temperature contrast, ΔT_1 , used as input for thermal stress calculation obtained as a difference between the “hot” and the reference thermal models; E. Temperature contrast, ΔT_2 , used as input for thermal stress calculation obtained as a difference between the “hot” and the reference thermal models.

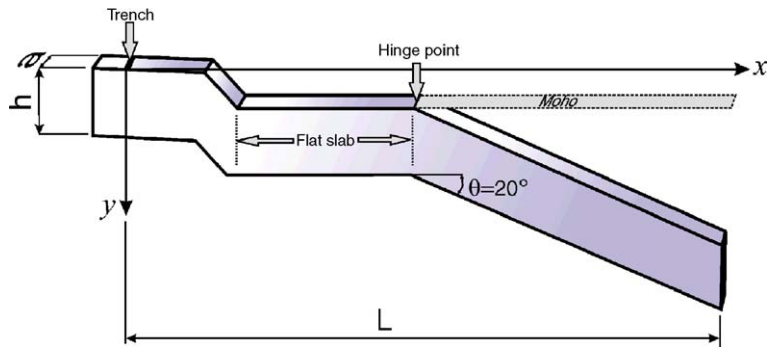


Fig. 5. Schematic representation for the subducting slab in Cartesian coordinates system. The origin is fixed on the slab surface at the trench. The plate is considered a thin slice with thickness, $h > a$ and length $L > a$. The slab dips into the asthenosphere at an angle $\theta = 20^\circ$.

the models incorporates frictional heating along the thrust fault (Fig. 2A). We used these two models to test the sensitivity of thermal stress on the temperature contrast, but the preferred model which is better constraints (Manea et al., 2004) is presented in Fig. 2A.

The slab geometry is constrained by gravity modeling (Kostoglodov et al., 1996), the location and extension of the coupled zones (Kostoglodov et al., 2003), local seismicity and the hypocenter location of the intraslab earthquakes (Fig. 1). The subducting Cocos plate presents two sharp bending points beneath the coast (Kostoglodov et al., 1996), then follows the ~ 150 km flat slab and finally the slab submerges into the asthenosphere at a dip angle of $\sim 20^\circ$ (Valdes et al., 1986) (Fig. 2).

The thermal stresses are caused by temperature variations ΔT which are measured relative to the temperature (T_i) at which the slab stress is zero (Turcotte and Schubert, 2002). Considering that the Cocos plate released the stress by slab flexure before entering in subduction, we choose as initial slab temperature (T_i) the oceanic geotherm corresponding to a 14 Ma oceanic plate (Cocos plate age at the trench from: Klitgord and Mammerickx, 1982; Kostoglodov and Bandy, 1995) (Fig. 3C). The final slab temperature distribution (T_f) is taken from the thermal models of Manea et al. (2004, 2005) (Fig. 3A,B). The non-uniform variation of slab temperature $\Delta T = T_f - T_i$ accounts for the thermal stresses in the subducted Cocos slab (Fig. 3D,E).

2.2. Two-dimensional formulation of thermal stress in thin plates

2.2.1. Basic principles

Here we present briefly the basic idea of thermal stresses, but the detailed discussion about the fundamental aspects of the thermal stress theory can be found

in Boley and Weiner (1997) and Timoshenko and Goodier (1951).

Thermal stresses arise in a heated/cooled slab due to a non-uniform temperature variation. We consider the slab made up of a number of small cubes with equal size bounded together to form a continuous body and also free of surface traction. In this case any uniform temperature variations would not produce any thermal stresses, because all the small cubes can expand/contract uniformly in all directions. On the contrary, if the temperature variation is non-uniform the small cubes will expand/contract by a different amount. Since the slab continuity must be satisfied, thermal stresses arise in this case. Such stresses can be separated in two parts (see Boley and Weiner (1997), p. 277): the first part is due to thermal expansion/contraction in areas with larger thermal gradients. The second part reflects upward/downward (convex/concave shape) of the slab, which induces an additional source of stress called thermal stress. The simple example shown in Fig. 4 illustrates these two types of stresses. We consider an unconstrained perfectly elastic plate, heated nonuniformly through its thickness only by an exponential temperature distribution. The dilatation of the slab top produces strong compressive stresses (high temperature gradients) at the top and relatively small tensional stresses at the bottom (low temperature gradients). Also, the slab bends upward (convex shape) because only the top of the slab is heated (expanded), producing tension at the top and compression at the bottom of the slab. The superposition of the two effects gives the following thermal stress pattern: compression at the top and bottom and tension in the slab core. Such peculiar stress pattern was also found in laboratory studies on nonuniform heated pine resin samples (Segawa et al., 1982). Also, Boley and Weiner (1997, p. 277) provide an analytical formulation for thermal stresses in thin

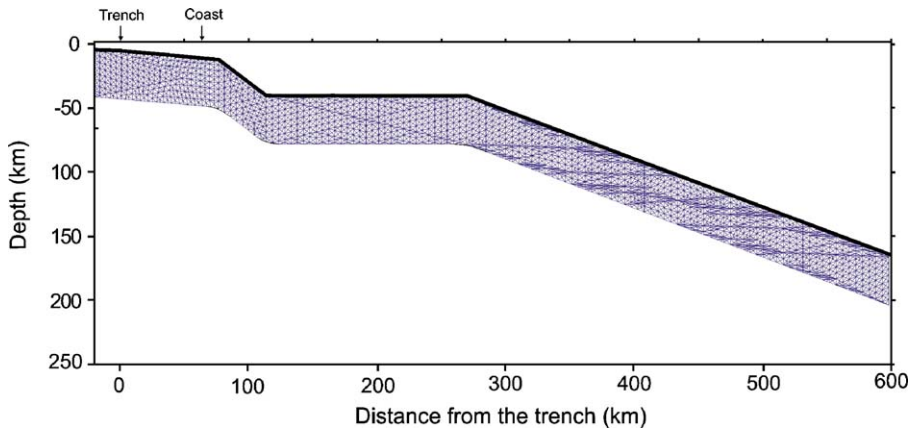


Fig. 6. A mesh with 5000 triangle shaped elements is used in thermal stress computation. The mesh resolution is about 3 km.

plates free of surface traction. For example, for an exponential temperature distribution through the plate thickness only, the same unusual stress pattern is obtained: compression at the top and bottom and tension in the plate core. If the bottom of the plate experiences high temperature it may yield by ductile flow, and the compression at the bottom is exponentially reduced.

2.2.2. Thermal stress models

We consider a 2D thermo-elastic problem where the temperature variation has the form $\Delta T = \Delta T(x, y)$ within a thin slice of the subducting slab with the thickness, $h \gg a$ and the length, $L \gg a$ (where a is the width) (Fig. 5). In this case the plane-stress formulation is assumed, therefore only one component of the normal stresses is zero, $\sigma_{xx} \neq 0$, $\sigma_{yy} \neq 0$ and $\sigma_{zz} = 0$ (Boley and Weiner, 1997; Turcotte and Schubert, 2002).

In the rectangular 2D Cartesian coordinate system (x, y) the 2D equations of equilibrium are obtained by considering the equilibrium of an infinitesimal parallelepiped (equilibrium of all the forces acting in the x and y directions) (Boley and Weiner, 1997):

$$\begin{cases} \frac{\partial \sigma_{xx}}{\partial x} + \frac{\partial \sigma_{xy}}{\partial y} = 0 \\ \frac{\partial \sigma_{xx}}{\partial x} + \frac{\partial \sigma_{yy}}{\partial y} = 0 \end{cases} \quad (1)$$

The stress–strain relations are:

$$\begin{cases} \epsilon_{xx} = \frac{1}{E}(\sigma_{xx} - \nu \sigma_{yy}) + \alpha \Delta T \\ \epsilon_{yy} = \frac{1}{E}(\sigma_{yy} - \nu \sigma_{xx}) + \alpha \Delta T \\ \epsilon_{xy} = \frac{\sigma_{xy}}{G} \end{cases} \quad (2)$$

The strain–displacement relations are:

$$\begin{cases} \epsilon_{xx} = \frac{\partial u}{\partial x} \\ \epsilon_{yy} = \frac{\partial v}{\partial y} \\ \epsilon_{xy} = \frac{1}{2} \left(\frac{\partial u}{\partial y} + \frac{\partial v}{\partial x} \right) \end{cases} \quad (3)$$

where the material properties are taken from Turcotte and Schubert (2002):

- α — coefficient of thermal expansion (10^{-5} – 3×10^{-5}) K^{-1} ;
- ν — Poisson’s ratio (0.23–0.25);
- E — Young’s modulus (60–80) GPa;
- G — $E/(1 + \nu)$;
- ΔT — temperature contrast = $T_i - T_f$.

The equilibrium equations (1) may be expressed in terms of strains (2); the strains in turn can be written in terms of displacements (3). The final result of these substitutions is the following equations in terms of displacements:

$$\begin{cases} \frac{E}{2(1-\nu)} \frac{\partial}{\partial x} \left(\frac{\partial u}{\partial x} + \frac{\partial v}{\partial y} \right) + \frac{E}{2(1+\nu)} \nabla^2 u - \frac{\alpha E}{1-\nu} \frac{\partial \Delta T}{\partial x} = 0 \\ \frac{E}{2(1-\nu)} \frac{\partial}{\partial y} \left(\frac{\partial u}{\partial x} + \frac{\partial v}{\partial y} \right) + \frac{E}{2(1+\nu)} \nabla^2 v - \frac{\alpha E}{1-\nu} \frac{\partial \Delta T}{\partial y} = 0 \end{cases} \quad (4)$$

The system of 2D equations (4) for thin plates is solved in term of displacements using the finite element solver PDE2D. The finite element grid extends from 20 km seaward of the trench up to 600 km landward. The lower limit of the model is considered the base of the oceanic lithosphere and corresponds to the 1150 °C

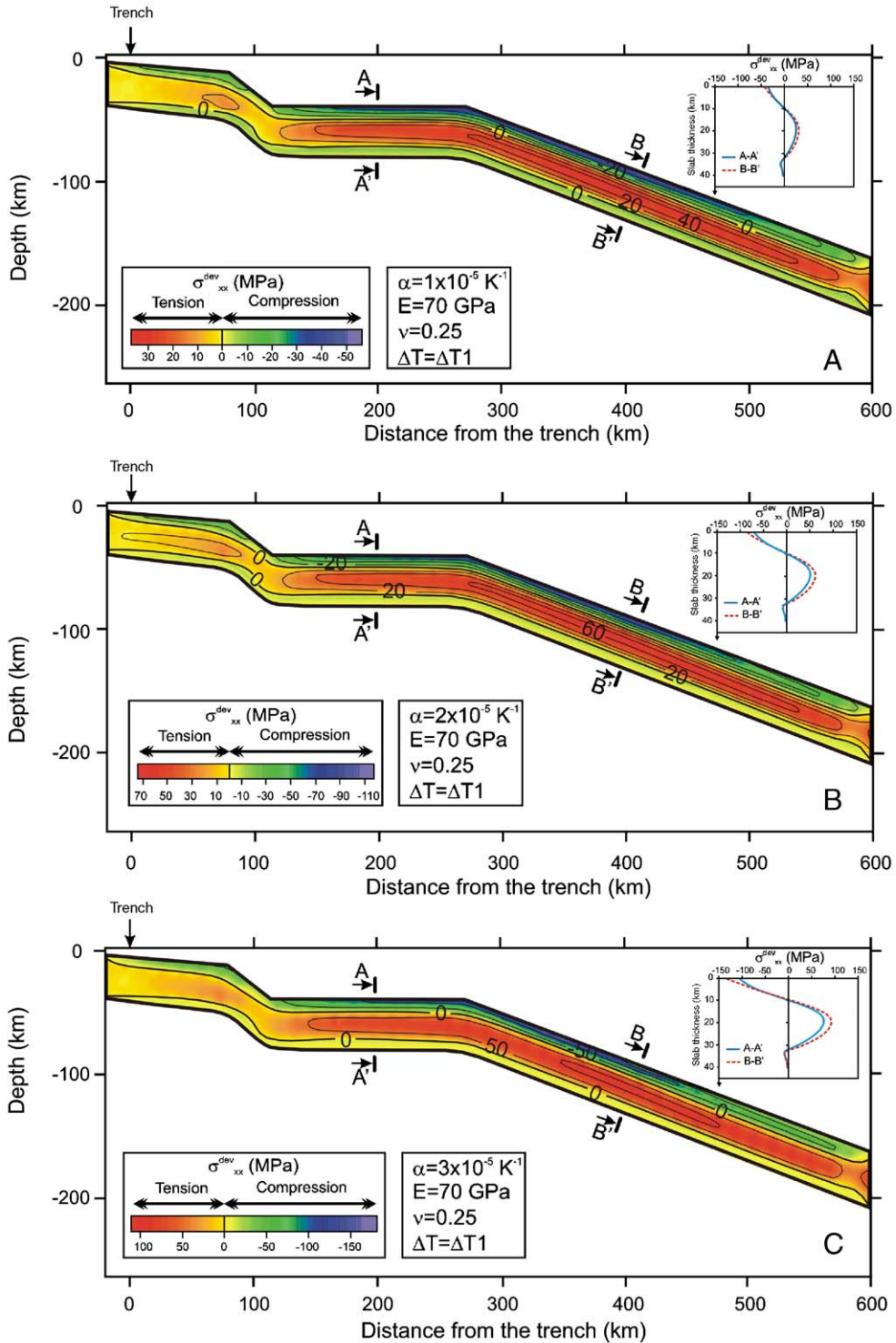


Fig. 7. The distribution of thermal stresses in the subducting Cocos plate beneath Central Mexico. The parameters used in the calculations are given in Table 1. Note the tensional slab core and the compressive slab top parallel with the slab dip.

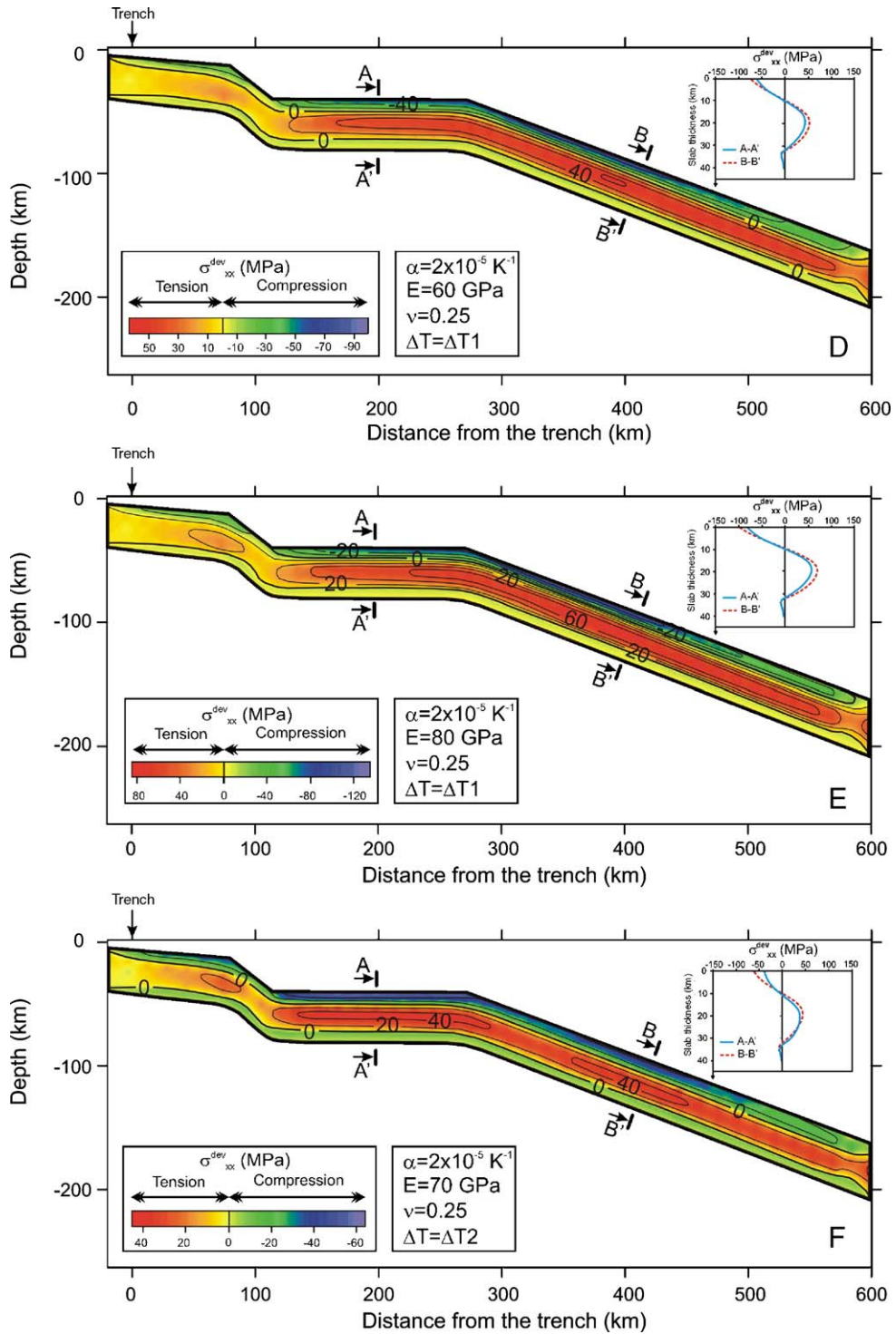


Fig. 7 (continued).

isotherm. The upper limit of the model is represented by the slab surface. The elastic parameters (E , ν and α) and temperature contrast (ΔT) are varied in order to quantify the sensitivity of the numerical models. We use free boundary of zero boundary forces in our model. The grid mesh is uniform and consists of 5000 triangle shaped elements (Fig. 6).

2.2.2.1. Deviatoric stresses. Considering $P_{\text{litho.}} = \rho gh$ as the confining lithostatic pressure, the resultant normal stresses are ($\sigma_{zz} = 0$ because of the plane-stress hypothesis):

$$\begin{cases} \sigma_{xx}^{\text{dev}} = \sigma_{xx} + P_{\text{litho.}} \\ \sigma_{yy}^{\text{dev}} = \sigma_{yy} + P_{\text{litho.}} \\ \sigma_{zz}^{\text{dev}} = P_{\text{litho.}} \end{cases} \quad (5)$$

Considering the mean stress $\bar{\sigma} = \frac{\sigma_{xx} + \sigma_{yy} + \sigma_{zz}}{3}$, the main deviatoric stresses is:

$$\sigma_{xx}^{\text{dev}} = \sigma_{xx} - \bar{\sigma} = \frac{2 \cdot \sigma_{xx} - \sigma_{yy}}{3} \quad (6)$$

2.2.2.2. Ductile creep at the bottom of the subducting slab. The thermal models (Fig. 2) show high temperatures (> 800 °C) at the lower part of the slab where temperature-activated creep is the dominant process (Burov and Diament, 1995). For our two-dimensional problem, we include the following relation for deviatoric yield stress for ductile creep (Watts, 2001):

$$\sigma_{xx}^{\text{dev}} = \sqrt[n]{\frac{\dot{\epsilon}}{A_p e^{\frac{-Q_p}{RT_f}}}} \quad (7)$$

The material constants adopted in this study are for dry olivine (Goetze, 1978; Kirby and Kronenberg, 1987):

- $n = 3$;
- A_p — power law stress constant = $7 \cdot 10^{-14}$ ($\text{Pa}^{-3} \text{s}^{-1}$);
- $\dot{\epsilon}$ — strain rate = 10^{-14} (s^{-1});
- Q_p — power law olivine activation energy = $520 \cdot 10^3$ (J/mol);
- R — universal gas constant = 8.31415 (J/mol K);
- T_f — slab temperature from Manea et al. (2004, 2005).

The deviatoric yield stress for ductile creep depends only on the absolute value of the temperature. The deviatoric thermal stress (6) at the bottom of the slab is replaced by the deviatoric yield for ductile creep (7)

wherever this is exceeded. In other words, the model is just elastic with a stress-cutoff using Eq. (7).

2.3. Gravity torque, suction torque and slab pull

The trenchward migration (in respect to the Middle American trench) of the Mexican volcanic arc for the last 7 Ma (Ferrari et al., 1999) reflects an increase of the slab dip through time beneath the arc. This observation suggests that the gravity torque should be larger than the suction torque. In this study we neglect the resistance forces (provided by the viscosity of the upper mantle) because they act mainly parallel to the slab and therefore they do not contribute significantly to the torque balance. We consider the slab to be a rigid body sinking into the asthenosphere with a constant speed of $u = 5.5$ cm/yr. Also, we assume that the mantle wedge has a uniform viscosity, η_{wedge} . With these assumptions, the suction torque (M_S) per unit trench length is (Stevenson and Turner, 1977):

$$M_S = 2\eta_{\text{wedge}}uL \left(\frac{\sin\theta}{(\pi-\theta) + \sin\theta} + \frac{\sin^2\theta}{\theta^2 - \sin^2\theta} \right) \quad (8)$$

where:

- η_{wedge} — mantle wedge viscosity (2×10^{19} – 4×10^{19} Pa s) (with an average of 3×10^{19} Pa s from Hirth and Kohlstedt, 2003)
- θ — slab dip angle (10° – 30° with an average $\sim 20^\circ$ from Valdes et al., 1986)
- u — convergence rate (5.5 cm/yr) (from model NUVEL 1A of DeMets et al., 1994)
- L — length of the subducting slab measured from the hinge point (150–350 km).

The gravitational torque (M_G) created by the density contrast $\Delta\rho$ between slab and the surrounding mantle is given by (Stevenson and Turner, 1977):

$$M_G = 0.5\Delta\rho gh_{\text{slab}}L^2 \cos\theta \quad (9)$$

where:

- g — gravity acceleration (10 m/s^2)
- h_{slab} — the slab thickness (40 ± 5 km)
- θ — slab dip angle (10° – 30° with an average $\sim 20^\circ$ from Valdes et al., 1986)
- L — length of the subducting slab measured from the hinge point (150–350 km).

The density increase $\Delta\rho$ between the subducting slab and the mantle is caused by two effects. First, the

transformation of hydrated basaltic oceanic crust (3400 kg/m³) to eclogite (3600 kg/m³) produces a density increase of $\Delta\rho_1 \sim 200 \text{ kg/m}^3$ in the upper 10 km of the subducted plate (Hacker et al., 2003). The second contribution in density increase ($\Delta\rho_2$) comes from the subducted lithosphere which is colder than the surrounding mantle and therefore denser (Turcotte and Schubert, 2002):

$$\Delta\rho_2 = \rho_m - \rho_m(1 - \alpha\Delta T) \quad (10)$$

where:

- ρ_m — mantle density (3325 kg/m³) (Sandwell, 2001)
- α — coefficient of thermal expansion ($1 \times 10^{-5} - 3 \times 10^{-5}$) K⁻¹ (Turcotte and Schubert, 2002)
- ΔT — average temperature contrast inside the slab 450 °C (Fig. 3A,B)

The total density increase is the weighted contribution from the two sources:

$$\Delta\rho = \Delta\rho_1 \cdot \frac{h_{\text{crust}}}{h_{\text{slab}}} + \Delta\rho_2 \cdot \frac{h_{\text{slab}} - h_{\text{crust}}}{h_{\text{slab}}} \quad (11)$$

where:

- h_{crust} — the oceanic crust thickness (10 km) (Sandwell, 2001)
- h_{slab} — the slab thickness (40 km).

The slab pull force (S_{pull}) created by the density contrast $\Delta\rho$ between slab and the surrounding mantle is given by

$$S_{\text{pull}} = \Delta\rho g h_{\text{slab}} L \sin\theta \quad (12)$$

3. Modeling results

3.1. Thermal stresses

The thermal stress calculations (deviatoric normal stresses σ_{xx}) are presented in Fig. 7. We take normal

stresses to be positive for tension and negative for compression. The obtained thermal stress pattern is as follows: the top and bottom of the subducting slab are in a compressive state while the core of the slab shows a tensional state. The areas of tensional and compressive stresses are parallel with the dip of the subducting slab. The lower part of the slab shows very low compressive stresses because the thermal stress is relieved by ductile flow at high temperature (>800 °C). The magnitude of the thermal stresses depends on the parameters used. We performed the sensitivity test presented in Table 1.

The test shows that the most important parameter for thermal stress is the coefficient of thermal expansion (α). The thermal stresses with $\alpha = 3 \times 10^{-5} \text{ K}^{-1}$ are with $\sim 300\%$ superior than for $\alpha = 1 \times 10^{-5} \text{ K}^{-1}$. The first part of the slab (distances < 115 km from the trench) reveals very small thermal stresses due to a small temperature contrast of less than 200 °C. The flat slab shows compressive stresses up to 110 MPa at the top, and tensional stresses up to 80 MPa in the slab core. The last segment of the subducting slab, which dips at nearly 20° into the asthenosphere, exposes high thermal stresses of $\sim 50-160 \text{ MPa}$ at the top and $\sim 40-90 \text{ MPa}$ in the core (Fig. 7A,B,C).

The second parameter varied is the Young's modulus E . The results show that an increasing of E from 60 GPa to 80 GPa leads to an increase in thermal stresses by $\sim 20\%$. The compression stresses on the top of the slab increase from $\sim 60 \text{ MPa}$ for the flat part up to 100 MPa at $\sim 100 \text{ km}$ depth. The tensional stresses in the core increases also with depth, from 50 MPa for the flat slab to 70 MPa at a depth of $\sim 100 \text{ km}$ (Fig. 7D,E).

We also test the sensitivity of our thermal-stress model in respect with the temperature field. We used the thermal model with no frictional heating and an isoviscous mantle wedge (Fig. 2B) from Manea et al. (2004). This model gives a temperature contrast with $\sim 200 \text{ °C}$ (on average) less than the previous thermal model. The results show a decrease in thermal stresses with $\sim 60\%$ (Fig. 7F). The last parameter tested here is the Poisson's ratio, ν . The thermal stresses response to Poisson ratio variation is less than $\sim 0.01\%$ and therefore is considered negligible.

Table 1
The parameters used to test the sensitivity of thermal stresses

$\alpha \text{ (K}^{-1}\text{)}$	1×10^{-5}	2×10^{-5}	3×10^{-5}	2×10^{-5}	2×10^{-5}	2×10^{-5}	2×10^{-5}	2×10^{-5}
$E \text{ (GPa)}$	70	70	70	60	80	70	70	70
$\nu \text{ (-)}$	0.25	0.25	0.25	0.25	0.25	0.24	0.26	0.25
$\Delta T \text{ (°C)}$	ΔT_1	ΔT_1	ΔT_1	ΔT_1	ΔT_1	ΔT_1	ΔT_1	ΔT_2

ΔT_1 — temperature contrast using the temperature-dependent viscosity (Fig. 3D).

ΔT_2 — temperature contrast using an isoviscous mantle wedge (Fig. 3E).

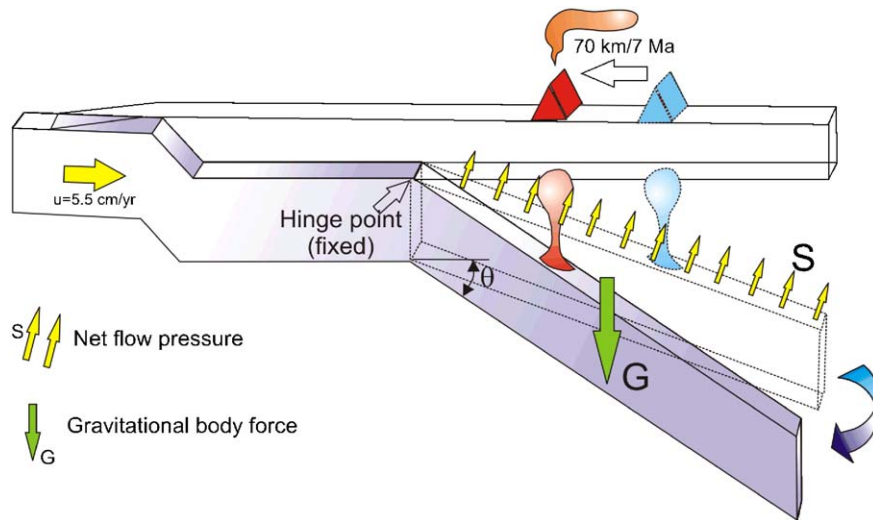


Fig. 8. The trenchward migration of the Mexican Volcanic Arc for the last 7 Ma suggests that the slab sinks into the asthenosphere at a bigger dip angle through time. The gravity body force, G , should exceed the net flow pressure, S , the slab acting like a lever attached to the flat slab at the hinge point plane.

3.2. Torque balance and slab pull

The above results show that the upper part of the flat slab is characterized by maximum thermal compressive stress of 40–100 MPa, depending on the elastic constants and input thermal model (Fig. 7). Such compressional stresses at the top of the subducting slab are not consistent with the exclusively normal fault intraslab earthquakes in Central Mexico. We propose here a mechanism which can compensate the compressional thermal stresses at the top of the flat slab by introducing a tensional state of stress in this region. This idea comes from the observation of trenchward migration of the Mexican volcanic arc for the last 7 Ma (Ferrari et al., 1999). This suggests that the gravity torque should be higher than the suction torque, so the slab sinks into the asthenosphere at bigger dip angles through time. In this case, we propose that the sinking Cocos plate would act like a lever, introducing a net clockwise

torque ($\Delta M = M_G - M_S > 0$) on the flat slab (Fig. 8). The gravity torque depends on density contrast inside the slab and slab length, whereas the suction force is a function of mantle wedge viscosity and slab length. The density contrast estimations using Eq. (11) are presented in Table 2. The results show a min/max density contrast ~ 56 – 89 kg/m^3 . Using dynamic models for Stokes flow for Tonga–Kermadec subduction zone, Billen and Gurnis (2001) obtained a density anomaly in the slab of 80 kg/m^3 . Also a recent study of Billen et al. (2003) uses a density anomaly within the slab of $\sim 66 \text{ kg/m}^3$. Kincaid and Hall (2003) used in their mantle flow models a density contrast of 2.9% (or $\sim 96 \text{ kg/m}^3$ assuming a mantle density of 3325 kg/m^3). Our estimates for density contrast inside the slab (56 – 89 kg/m^3) are in good agreement with the above studies (66 – 96 kg/m^3). In this study we use a density anomaly of $75 \pm 20 \text{ kg/m}^3$.

It is difficult to provide an exact estimate for the mantle wedge average viscosity, because it depends on many parameters like: pressure, temperature, differential stress and water content, which in turn can vary considerably from one subduction zone to another. However, Hirth and Kohlstedt (2003) provide a mean value of $3 \times 10^{19} \text{ Pa s}$ for olivine aggregates with a water content of $500 \text{ H}/10^6 \text{ Si}$, a temperature of $1200 \text{ }^\circ\text{C}$, a pressure of 1.0 GPa and a differential stress of 0.3 MPa . Armstrong and Calderwood (1998) suggest a mantle wedge viscosity of $2 \times 10^{19} \text{ Pa s}$, and Billen and Gurnis (2001) used a low viscosity wedge

Table 2

The density contrast estimations using Eq. (11) provide a $\Delta\rho_{\text{min}} = 56 \text{ kg/m}^3$ and a $\Delta\rho_{\text{max}} = 89 \text{ kg/m}^3$. In this study we use a $\Delta\rho = 75 \pm 20 \text{ kg/m}^3$, which is consistent with our estimates and also with previous published estimates

h_{slab} (km)	35	40	45
α ($^\circ\text{C}^{-1}$)			
1×10^{-5}	67.9	61.2	56.1
2×10^{-5}	78.6	72.5	67.7
3×10^{-5}	89.3	83.8	79.4

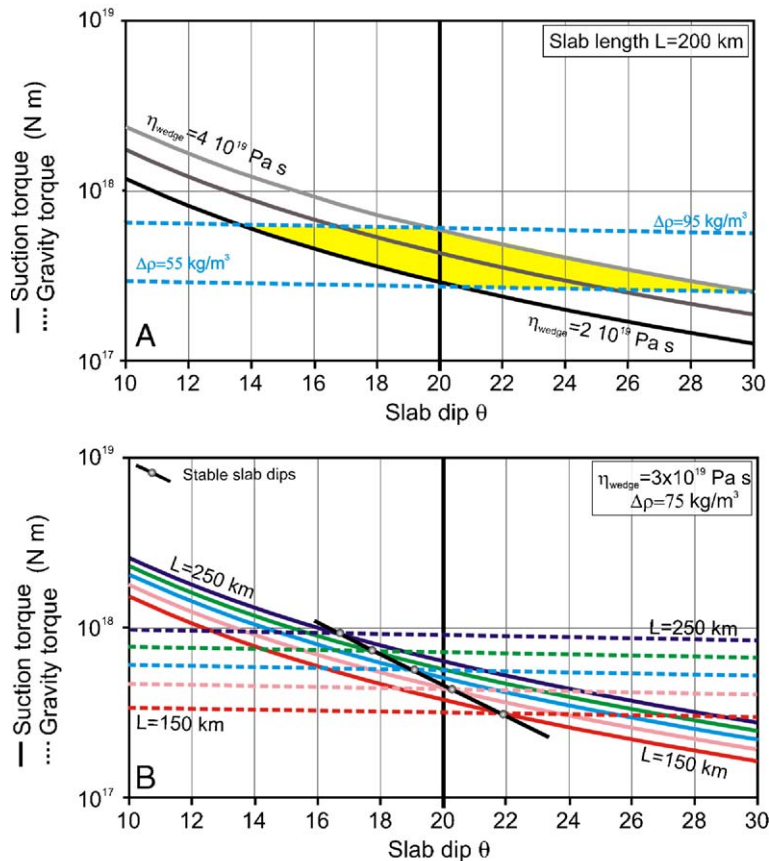


Fig. 9. The gravity torques plotted as function of angle of subduction, θ , mantle wedge viscosity, η_{wedge} . Intersection between gravity and suction torques gives the stable slab dip. A. For a density contrast of $75 \pm 20 \text{ kg/m}^3$ and a slab length of 200 km, the present day dip angle $\theta = 20^\circ$ is plausible for viscosities of $2 \times 10^{19} - 4 \times 10^{19} \text{ Pa s}$. B. For a mantle wedge viscosity of $3 \times 10^{19} \text{ Pa s}$ and the density contrast of 75 kg/m^3 , a $19 \pm 3^\circ$ slab dip is realistic for slab lengths of $200 \pm 50 \text{ km}$.

($3 \times 10^{19} \text{ Pa s}$) in order to fit the modeled gravity and geoid with the observations, for the Tonga–Kermadec subduction zone. Also, Cathles (1975) argues that there could be a narrow channel, 75 km thick just beneath the lithosphere, with a viscosity of $4 \times 10^{19} \text{ Pa s}$. Based on these estimates, we assume in this study a mantle wedge viscosity $2 \times 10^{19} - 4 \times 10^{19} \text{ Pa s}$. Although we are interested in the difference between gravity and suction torques, we perform a sensitivity test to investigate if a $\sim 20^\circ$ slab dip would be realistic within the above density contrasts and mantle wedge viscosity estimates. The results of the sensitivity test (Fig. 9A) show that for a slab length of 200 km, the slab dip varies from $22^\circ \pm 8$. If we fix the wedge viscosity at $3 \times 10^{19} \text{ Pa s}$ and the density contrast to an average of 75 kg/m^3 , then we obtain stable slab dips of $19^\circ \pm 3^\circ$ for the slab lengths of $200 \pm 50 \text{ km}$ (Fig. 9B). The suction and gravity torques estimates are somewhat large, because they are directly proportional to the mantle wedge viscosity, slab density

contrast and slab length uncertainties. For a dip angle of 20° , a slab length of 200 km and viscosities from $2 \times 10^{19} \text{ Pa s}$ to $4 \times 10^{19} \text{ Pa s}$, the suction torque varies from $\sim 5 \times 10^{17} \text{ N m}$ to $\sim 8 \times 10^{17} \text{ N m}$ (Fig. 9A). Also, for slab lengths of 150–250 km (dip angle of 20° and a mantle viscosity of $3 \times 10^{19} \text{ Pa s}$) the suction torque varies from $\sim 6 \times 10^{17} \text{ N m}$ to $\sim 8 \times 10^{17} \text{ N m}$ (Fig. 9B). The gravity torque uncertainties are similar to those for suction torque if we assume a density contrast of $70 \pm 25 \text{ kg/m}^3$ (Fig. 9A). However, the gravity torque is more sensitive to slab length uncertainties. Slab length variations from 150 km to 250 km induce a half order of magnitude uncertainty for the gravity torque ($5 \times 10^{17} - 10^{18} \text{ N m}$) (Fig. 9B).

The intersection between the gravitational and suction torque gives a stable slab dip. However, any slight difference between the suction and gravity torques would make the slab to lift or to sink into the surrounding mantle (Fig. 10). Assuming that the slab sinks into the mantle, we

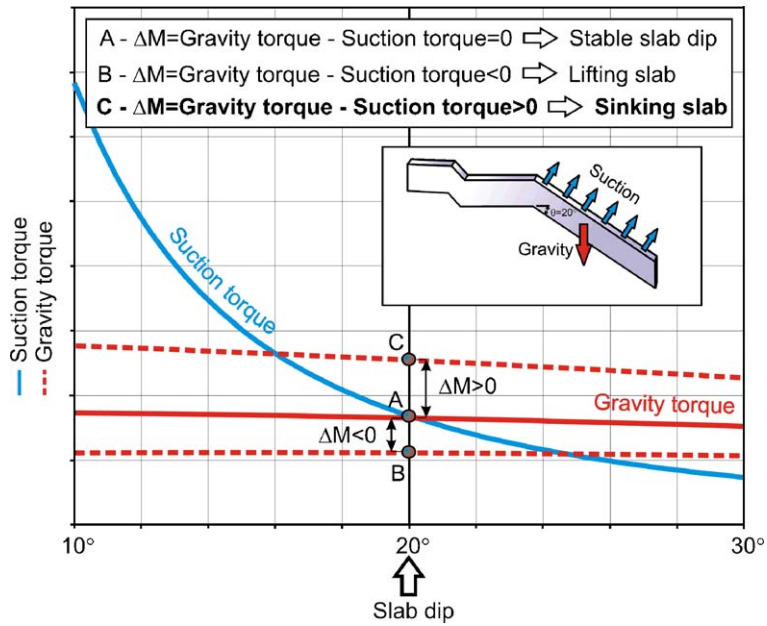


Fig. 10. Gravitational versus suction torque. If the two torques are equal, then the subducting slab dips into the asthenosphere at a constant θ . Any slight deviation from the balance would make the slab to lift or to sink into the surrounding mantle.

calculate the net torque ΔM which induces a tensile stress in the upper part of the slab, and therefore might compensate the maximum compressive thermal stresses on the

top of the flat slab (40–110 MPa). We treat the flat slab like an embedded plate subject to an applied clockwise torque ΔM (Fig. 11A). The relation between this torque

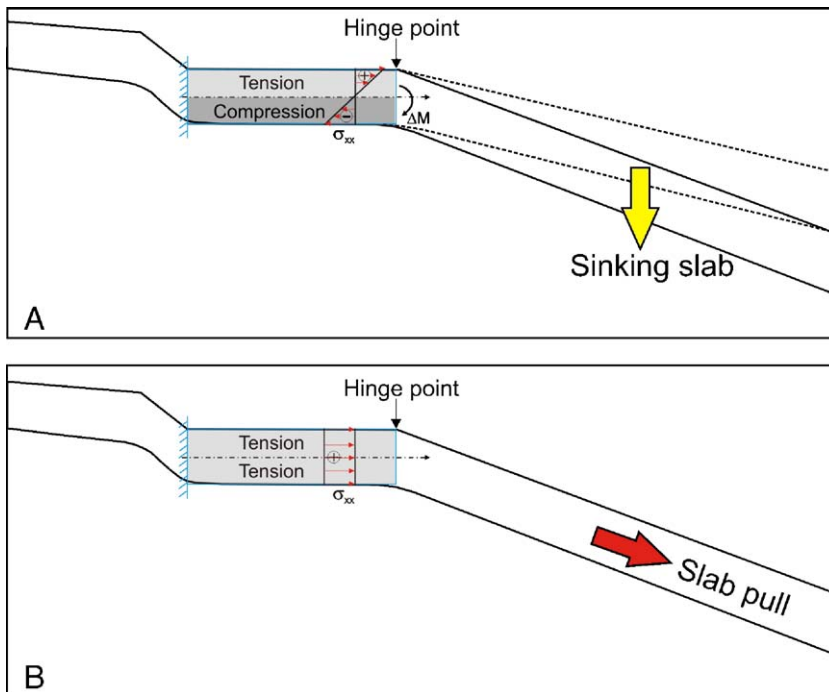


Fig. 11. A. The sinking slab induces a clockwise torque (ΔM) at one end of the flat slab. The flat slab is treated as an embedded plate subject to an applied clockwise torque ΔM . The upper half of the flat slab is extended and the lower half is contracted. B. The slab pull force created by the negative buoyancy of the sinking slab induces a constant tensile stress in the flat segment.

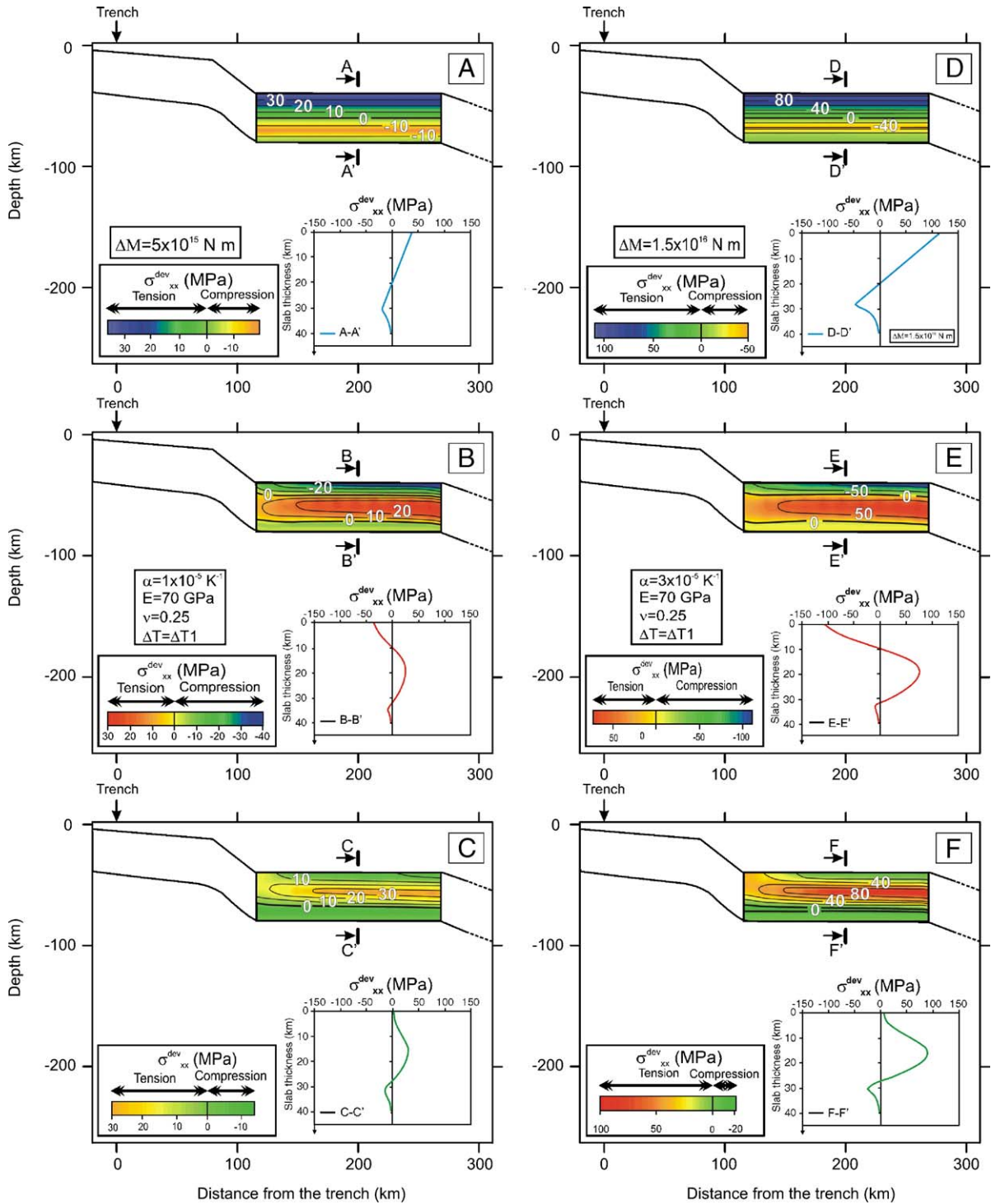


Fig. 12. Linear superposition of the torque induced stresses (A and D) and thermally induced stresses (B and E) for the flat slab for two different coefficients of thermal expansion α ($1 \times 10^{-5} \text{ K}^{-1}$ and $3 \times 10^{-5} \text{ K}^{-1}$). The results (C and F) show a stress pattern which now consists in tensional stresses for the top and core of the flat slab from 30 MPa using a low value for α of $1 \times 10^{-5} \text{ K}^{-1}$ and up to 90 MPa for α of $3 \times 10^{-5} \text{ K}^{-1}$.

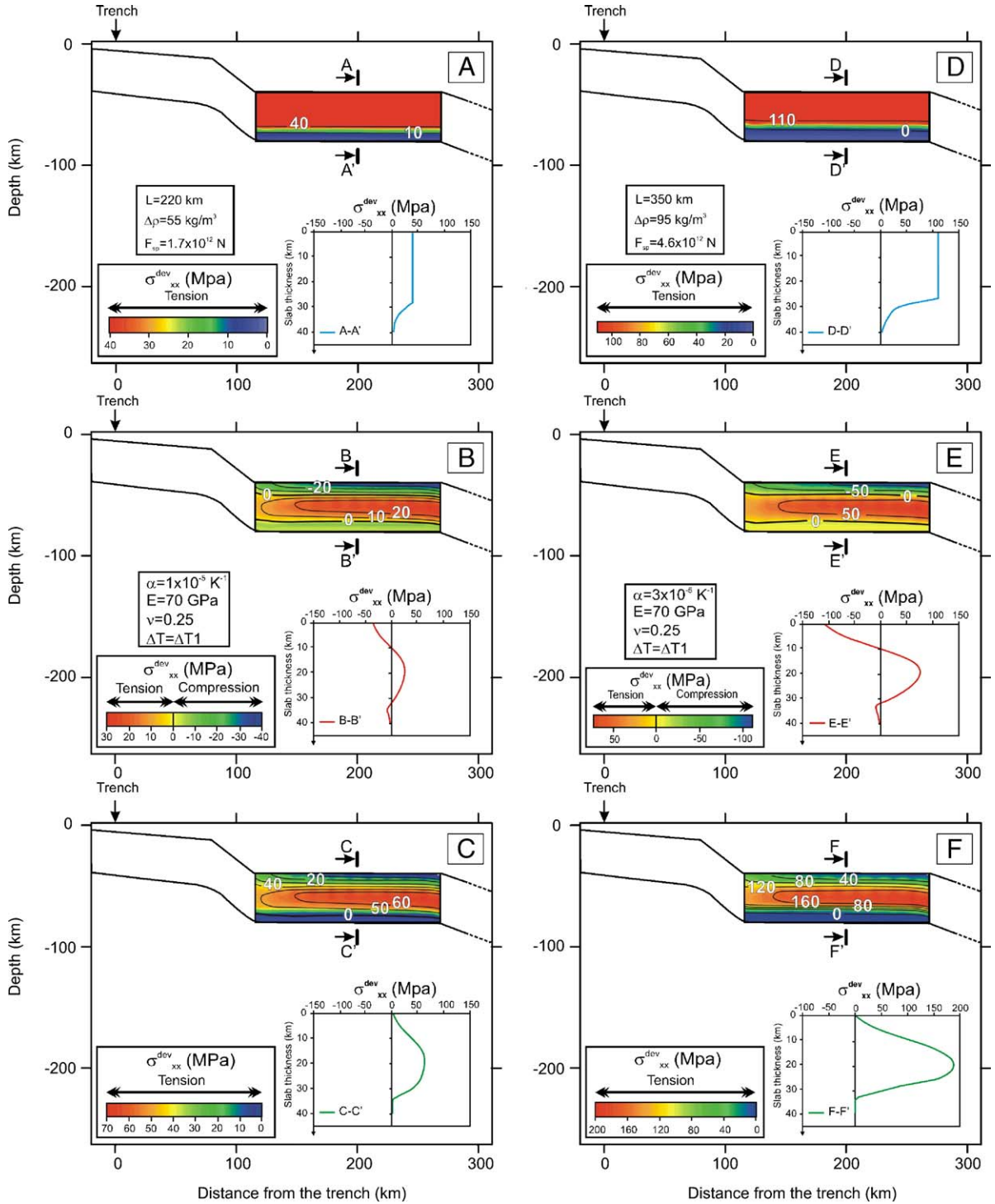


Fig. 13. Linear superposition of the slab pull induced stresses (A and D) and thermally induced stresses (B and E) for the flat slab for two different coefficients of thermal expansion α ($1 \times 10^{-5} \text{ K}^{-1}$ and $3 \times 10^{-5} \text{ K}^{-1}$). The results (C and F) show a stress pattern which now consists in pure tensional stresses for the entire flat slab (60–180) MPa.

and the stresses over the cross section of the slab of thickness h is given by (Turcotte and Schubert, 2002):

$$\Delta M = \int_{-h/2}^{h/2} \sigma_{xx} y dy$$

$$\sigma_{xx} = \frac{E}{(1-\nu^2)} \epsilon_{xx} \quad (13)$$

Assuming small deflection of the flat slab, the stress σ_{xx} produced by the net torque ΔM is obtained as following (Turcotte and Schubert, 2002):

$$\epsilon_{xx} = -y \frac{d^2 w}{dx^2} \Rightarrow \Delta M = \frac{-Eh^3}{12y(1-\nu^2)} \frac{d^2 w}{dx^2} = \frac{Eh^3}{12y(1-\nu^2)} \epsilon_{xx} \Rightarrow \sigma_{xx} = \frac{12\Delta M}{h^3} y \quad (14)$$

We also include the ductile creep at the bottom of the flat slab in the same manner as for thermal stresses. The results are presented in Fig. 12A,B where the top half of the flat slab has tensile stresses of 40–110 MPa, whereas the bottom is in compression (20–60 MPa) where the stresses decrease asymptotically to zero due to

creep flow. The neutral plane is located in the middle of the plate. These stresses correspond to small values of net torque ΔM of 0.5×10^{16} – 1.5×10^{16} N m.

An alternative source of tensile stresses is the slab pull force caused by the negative buoyancy of the subducting slab. Using a density contrast of 55 kg/m^3 and a slab length of 220 km, a 20° dip angle would produce a slab pull of 1.7×10^{12} N per unit trench length. This force produces a tensile stress of ~ 41 MPa in the 40 km thick flat slab (Fig. 13A). This tensional stress is sufficient to compensate the lower compressional thermal stress estimate of 40 MPa (Fig. 13B), and put the whole flat slab in tension (Fig. 13C). To balance the higher compressional thermal stress (110 MPa) we use a density contrast of 95 kg/m^3 and a slab length of 350 km. This would produce a slab pull of 4.6×10^{12} N (114 MPa) per unit trench length for a 20° dip angle (Fig. 13DEF).

4. Intraslab seismicity and stress pattern

The intraslab seismicity in Guerrero is characterized by shallow to intermediate depth (<90 km) intraslab normal fault earthquakes (Fig. 1). Most of the events

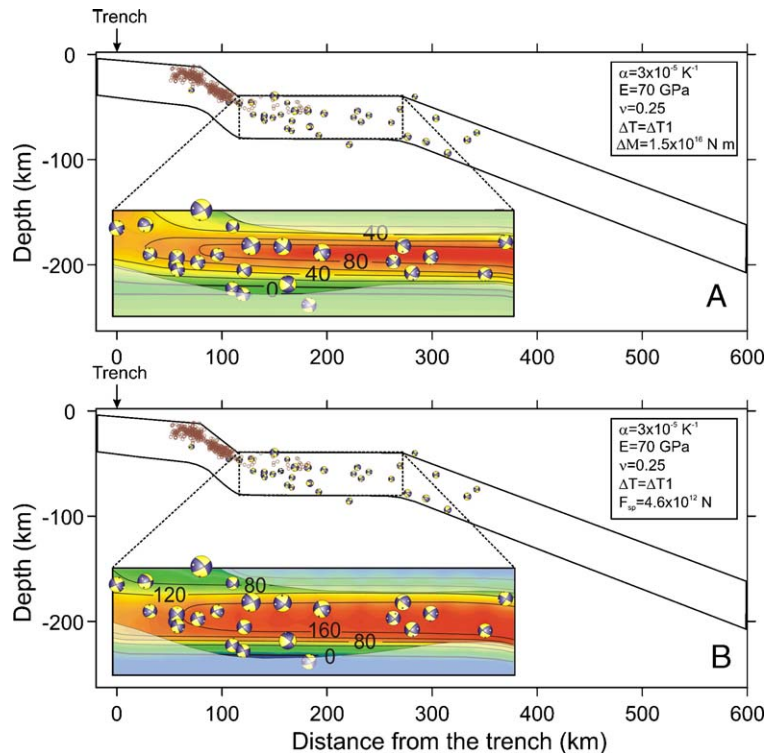


Fig. 14. A good correlation between the tensile stress pattern (Figs. 12F and 13F) and the intraslab hypocenters inside the flat slab can be observed. The majority of the flat slab hypocenters lie where the slab exhibits tensional stresses superior of 40 MPa (A) or 80 MPa (B). The transparent envelope is used only to enhance the good correlation between the stress distribution and intraslab earthquake location.

(~ 90%) are confined in the subhorizontal part of the slab (115–270 km distance from the trench). Two clusters of events, representing the background seismic activity with low magnitude ($M_w < 4$), are presented also (small circles in Fig. 2), and they appear to be related to the sharp bending–unbending of the plate at ~ 80 km and ~ 110 km from the trench. According to Manea et al. (2004), significant deviatoric stresses up to several MPa are expected in these sharp bending points. Strong earthquakes should accompany such large stresses, but in reality numerous small events clustered in two clouds seems to be the response of the subducting Cocos plate to bending–unbending. The study of such peculiar behavior is beyond the scope of this paper; therefore we did not include in our calculation such stresses. The maximum depth extent of the present models (Fig. 2) is 200 km, therefore the effect of olivine–spinel phase change on the stress distribution of the subducting slab is not included here. Also, the transmitted ridge push, is not incorporated in the modeling.

The thermal stress calculations show a tensional ~ 20 km thick slab core with deviatoric stresses up to 40–80 MPa. This state of stress is consistent with the normal fault intraslab seismicity. However, the top of the slab is characterized by significant compressional thermal stress up to 110 MPa although thrust earthquakes have not been recorded in this region.

Using the torque calculations described in the previous chapters, we linearly superimposed the thermal stresses and torque stresses for the flat slab (Fig. 12). The results show a stress pattern which now consists in tensional stresses for the top and core of the flat slab from 30 MPa (Fig. 12C) for a low value for α of $1 \times 10^{-5} \text{ K}^{-1}$ and up to 90 MPa for α of $3 \times 10^{-5} \text{ K}^{-1}$ (Fig. 12F). At the bottom of the slab, the compressional stresses decrease exponentially to zero due to creep flow at high temperature.

Combining the slab pull stresses of 41–114 MPa with the thermal stresses, we also obtained pure tensional stresses (60–180 MPa) inside the flat slab (Fig. 13CF).

A good correlation between the tensile stress pattern and the intraslab hypocenters inside the flat slab can be observed in Fig. 14. The majority of the intraslab earthquakes are placed inside the slab core, where the resultant tensile stresses are above ~ 40 MPa (Fig. 14A) or ~ 80 MPa (Fig. 14B), although few of them lie down at higher depths where ductile flow is expected. This is probably because we use in this study intraslab earthquakes which are located far from our 2D cross-section

(Fig. 1), where the flat slab might be located at slightly different depths than beneath Guerrero.

5. Discussion and conclusions

Based on the newly developed thermal models for Guerrero subduction zone (Manea et al., 2004), the thermal stress due to non-uniform temperature contrast ΔT in the subducting Cocos slab is calculated using a finite element approach. The slab was considered purely elastic, but we incorporate a ductile creep at the bottom of the slab for temperature larger than 800 °C. The temperature given by a 14 Ma slab geotherm (Cocos plate age at the trench in Central Mexico) was used as the initial temperature. A sensitivity test shows that the thermal stresses are very sensitive on the coefficient of thermal expansion α , slightly sensitive on Young's modulus E and temperature contrast ΔT , and negligible on the Poisson ratio ν .

The calculations show a ~ 20 km thick slab core in a tensional state with stresses up to 40–80 MPa. On the other hand, the top of the slab exposes compressive thermal stresses up to 110 MPa depending on location and elastic parameters (Fig. 7). The magnitude of the compressional stresses at the top of the slab are with ~ 30% higher than for the lower part when no ductile flow is included at the bottom of the slab. This reflects a higher thermal gradient in the temperature contrast at the top of the slab (Fig. 3D-inset). However, the ductile flow reduces considerably the compressive stresses at the bottom of the slab, and they can be considered negligible (Fig. 7).

The compressional stresses at the top of the slab are inconsistent with the exclusively normal fault character of the intraslab earthquakes in Central Mexico, and therefore an additional opposite stress source might exist. The migration of the Mexican volcanic arc toward the trench in the last 7 Ma (Ferrari et al., 1999) suggest that the subducting Cocos slab has been increasing its dip through time. In this case, the gravity torque should be higher than the suction torque, the descending Cocos plate acting like a lever attached to the subhorizontal slab. A net torque of 0.5×10^{16} – 1.5×10^{16} N m induces tensile stress in the upper half comparable with the compressional thermal stresses. The superposition of the thermal and torque stresses confers a purely tensional state (40–90 MPa) of stress in the flat slab which is consistent with the normal fault intraslab events (Fig. 12).

An alternative manner to eliminate the compressional thermal stresses in the flat slab is to exploit the negative buoyancy of the sinking slab. A slab pull force of 1.7×10^{12} – 4.6×10^{12} N per unit trench length, created by a density anomaly of 55–95 kg/m³, induces a tensional

stress of 41–114 MPa, sufficient to compensate the compressive thermal stresses at the top of the flat slab (40–110 MPa). Our results agree well with previous studies of slab pull estimates, $\sim 4.5 \times 10^{12}$ N/m (Bott, 1993) and $\sim 4.1\text{--}6.1 \times 10^{12}$ N/m (Schellart, 2004). These slab pull values should be considered as minimum estimates for Central Mexico. The combination between slab pull and thermal stresses provides a pure compressional stress pattern with stresses up to 180 MPa in the flat slab core (Fig. 13F).

In this study, our calculations are based on several simplifications. We did not include in the models stresses generated by phase transitions and bending–unbending. The intraslab seismicity cuts off at ~ 100 km depth (Fig. 2), and the slab dip used in this study is just an extrapolation. According to Manea et al. (2005) the exothermic phase transition in the subducting oceanic crust from basalt to eclogite occurs between 60 km to 80 km depth in Central Mexico. Such a phase transition might affect the state of stress in the descending slab in two ways: first, the density increase results in a contraction and therefore in an increased compressive stress; second, the denser material acts like an additional load that pulls down the slab. We did not include in our models here the first effect, because this would lead to a more increase of the compressive stress at the top of the slab, which is already inconsistent with the normal fault intraslab earthquakes in Central Mexico. Also the bending–unbending at the sharp points beneath the cost is not included here, because the response of the subducting Cocos plate is very unexpected and represented by intense microseismicity instead of large earthquakes as might be anticipated. However, all these effects might have a minor influence on the long flat slab, where thermal expansion can be the dominant source of stresses.

At the first order, the superposition of the stress sources considered in this study (thermal and torque or slab pull induced) explains the existence of exclusively normal faults intraslab earthquakes in the flat slab beneath Mexico. Furthermore, our calculations show that thermal stresses due to non-uniform reheating of subducting slabs may play a considerable role on the total state field, with thermal stresses inside the slab core as high as 160 MPa.

Acknowledgments

Helpful critical comments and constructive suggestions by Patrick Scheffmann, Kevin Furlong, Jeroen van Hunen, and one anonymous reviewer were used to improve the manuscript. This study was supported by CONACYT (Consejo Nacional de Ciencia y Tecnología) Grants G25842-T and 37293-T and by PAPIIT (Programa de Apoyo a Proyectos de Investigación e Innovación

Technológica) Grant IN104801. We also like to acknowledge support from the Gordon and Betty Moore Foundation. This is a contribution 9145 of the Division of Geological and Planetary Sciences, CALTECH.

References

- Armstrong, R.L., Calderwood, A.R., 1998. Constraints on the Earth's viscosity from a frequency, temperature and pressure dependent mantle Q: the viscosity model. EOS Transactions AGU 79 (45), F885 (Fall Meet. Suppl.).
- Billen, M.I., Gurnis, M., Simons, M., 2003. Multiscale dynamics of the Tonga–Kermadec subduction zone. *Geophysical Journal International* 153, 359–388.
- Billen, M.I., Gurnis, M., 2001. A low viscosity wedge in subduction zones. *Earth and Planetary Science Letters* 193, 227–236.
- Boley, B.A., Weiner, J.H., 1997. *Theory of Thermal Stresses*, 1st Edition. Dover Publications, INC., Mineola, New York.
- Bott, M.H.P., 1993. Modelling the plate-driving mechanism. *Journal of the Geological Society, London* 150, 941–951.
- Bratt, S.R., Bergman, E.A., Solomon, S.C., 1985. Thermoelastic stress: how important as a cause of earthquakes in young oceanic lithosphere. *Journal of Geophysical Research* 90, 10249–10260.
- Burov, E.B., Diament, M., 1995. The effective elastic thickness (T_e) of continental lithosphere: what does it really mean? *Journal of Geophysical Research* 100 (B3), 3905–3927.
- Cathles, L.M., 1975. *Viscosity of the Earth's Mantle*. Princeton University Press, Princeton. 403 pp.
- Collette, B.J., 1974. Thermal contraction joints in a spreading seafloor as origin of fracture. *Nature* 252, 299–300.
- Conder, J.A., Weins, D.A., Morris, J., 2002. On the decompression melting structure at volcanic arcs and back-arc spreading centres. *Geophysical Research Letters* 29, 171–174.
- Dean, B.W., Drake, C.L., 1978. Focal mechanism solutions and tectonics of the Middle America arc. *Journal of Geology* 86, 111–128.
- DeMets, C., Gordon, R., Argus, D., Stein, S., 1994. Effect of recent revisions to the geomagnetic reversal time scale on estimates of current plate motions. *Geophys. Res. Lett.* 21, 2191–2194.
- Engdahl, E.R., Villaseñor, A., 2002. Global seismicity: 1900–1999. In: Lee, W.H.K. (Ed.), *International Handbook of Earthquake Engineering and Seismology*, International Geophysics Series, vol. 81A, pp. 665–690.
- Ferrari, L., Lopez-Martinez, M., Aquirre-Diaz, G., Carrasco-Nunez, G., 1999. Space–time patterns of Cenozoic arc volcanism in Central Mexico: from Sierra Madre Occidental to the Mexican Volcanic Belt. *Geology* 27 (4), 303–306.
- Furukawa, F., 1993. Magmatic processes under arcs and formation of the volcanic front. *Journal of Geophysical Research* 98, 8309–8319.
- Goetze, C., 1978. The mechanisms of creep in olivine. *Philosophical Transactions of the Royal Society of London. A* 288, 99–119.
- González-Ruiz, J.R., 1986. Earthquake source mechanics and tectonophysics of the middle America subduction zone in Mexico. Ph.D. Thesis, Univ. of Calif., Santa Cruz.
- Gonzalez-Ruiz, J.R., McNally, K.C., 1988. Stress accumulation and release since 1882 in Ometepe, Guerrero, Mexico: implications for failure mechanisms and risk assessments of a seismic gap. *Journal of Geophysical Research* 93, 6297–6317.
- Gorbatov, A., Kostoglodov, V., Suárez, G., Gordeev, E., 1997. Seismicity and structure of the Kamchatka subduction zone. *Journal of Geophysical Research* 102, 17,883–17,898.

- Goto, K., Hamaguchi, H., Suzuchi, Z., 1985. Earthquake generating stresses in the descending slab. In: Kobayashi, K., Sacks, I.S. (Eds.), *Structures and Processes in the Subduction Zones* Tectonophysics, vol. 112, pp. 111–128.
- Hacker, B.R., Abers, G.A., Peacock, S.M., 2003. Subduction factory. 1. Theoretical mineralogy, densities, seismic wave speeds, and H₂O content. *Journal Geophysical Research* 108. doi:10.1029/2001JB001127.
- Hamaguchi, H., Goto, K., Suzuki, Z., 1983. Double-planned structure of intermediate-depth seismic zone and thermal stress in the descending plate. *Journal of Physics of the Earth* 331, 329–347.
- Haxby, W.F., Parmentier, E.M., 1988. Thermal contraction and the state of stress in the oceanic lithosphere. *Journal of Geophysical Research* 93, 6419–6429.
- Hirth, G., Kohlstedt, D.L., 2003. Rheology of the mantle wedge. In: Eiler, J. (Ed.), *Inside the Subduction Factory*, Geophysical Monograph, vol. 138. AGU, Washington DC, pp. 83–105.
- Iglesias, A., Singh, S.K., Pacheco, J.F., Ordaz, M., 2002. A source and wave propagation study of the Copalillo, Mexico earthquake of July 21, 2000 (Mw=5.9): implications for seismic hazard in Mexico City from inslab earthquakes. *Bulletin of Seismological Society of America* 92 (3), 1060–1071.
- Jiménez, Z., Ponce, L., 1978. Focal mechanism of six large earthquakes in northern Oaxaca, Mexico, of the period 1928–1973. *Geofísica Internacional* 17, 379–386.
- Jischke, M.C., 1975. On the dynamics of descending lithospheric plates and slip zones. *Journal of Geophysical Research* 80 (35), 4809–4813.
- Kelemen, P.B., Rilling, J.L., Parmentier, E.M., Mehl, L., Hacker, B.R., 2003. Thermal structure due to solid-state flow in the mantle wedge beneath arcs inside the subduction factory. In: Eiler, J. (Ed.), *Geophysical Monograph*, vol. 138. AGU, Washington, pp. 293–311.
- Kincaid, C., Hall, C., 2003. Role of back arc spreading in circulation and melting at subduction zones. *Journal of Geophysical Research* 108 (B5), 2240. doi:10.1029/2001JB001174.
- Kirby, S.H., 2000. Taking the temperature of slabs. *Nature* 403, 31–34.
- Kirby, S.H., Kronenberg, A.K., 1987. Rheology of the lithosphere: selected topics. *Reviews of Geophysics* 25, 1219–1244.
- Klitgord, K.D., Mammerickx, 1982. Northern east Pacific Rise; magnetic anomaly and bathymetric framework. *Journal of Geophysical Research* 87 (138), 6725–6750.
- Kostoglodov, V., Bandy, W.L., 1995. Seismotectonic constraints on the convergence rate between the Rivera and North American plates. *Journal of Geophysical Research* 100, 17977–17989.
- Kostoglodov, V., Bandy, W., Domínguez, J., Mena, M., 1996. Gravity and seismicity over the Guerrero seismic gap, Mexico. *Geophysical Research Letters* 23, 3385–3388.
- Kostoglodov, V., Singh, S.K., Santiago, J.A., Franco, S.I., Larson, K. M., Lowery, A.R., Bilham, R., 2003. A large silent earthquake in the Guerrero seismic gap, Mexico. *Geophysical Research Letters* 30 (15), 1807.
- Lay, T., Astiz, L., Kanamori, H., Christensen, D.H., 1989. Temporal variation on of large intraplate earthquakes in coupled subduction zones. *Physics of the Earth and Planetary Interiors* 54, 258–312.
- Lefevre, L.V., McNally, K.C., 1985. Stress distribution and subduction of aseismic ridges in the middle America subduction zone. *Journal of Geophysical Research* 90, 4495.
- Manea, V.C., Manea, M., Kostoglodov, Currie, C.A., Sewell, G., 2004. Thermal structure, coupling and metamorphism in the Mexican subduction zone beneath Guerrero. *Geophysical Journal International* 158, 775–784.
- Manea, V.C., Manea, M., Kostoglodov, V., Sewell, G., 2005. Thermo-mechanical model of the mantle wedge in Central Mexican subduction zone and a blob tracing approach for the magma transport. *Physics of the Earth and Planetary Interiors* 149, 165–186.
- Pardo, M., Suárez, G., 1995. Shape of the subducted Rivera and Cocos plates in southern Mexico: seismic and tectonic implications. *Journal of Geophysical Research* 100, 12357–12373.
- Poli, S., Schmidt, M.W., 2002. Petrology of subducted slabs. *Annual Review Earth Planetary Sciences* 30, 1–29.
- Sandwell, D.T. 2001. Crustal structure, isostasy and rheology. Web: http://topex.ucsd.edu/geodynamics/08crust_rheology.pdf.
- Schellart, W.P., 2004. Quantifying the net slab pull force as a driving mechanism for plate tectonics. *Geophysical Research Letters* 32, L07611. doi:10.1029/2004GL019528.
- Stevenson, D.J., Turner, J.S., 1977. Angle of subduction. *Nature* 270, 334–336.
- Segawa, S., Hamaguchi, H., Goto, K., 1982. A model experiment on the generating 694 stresses for the double-plane structure of the intermediate-depth seismic activity. *Zisin ser.2* (35), 19–34 (J. Seismol. Soc. Japan).
- Singh, S.K., Pardo, M., 1993. Geometry of the Benioff zone and the state of stress in the overriding plate in central México. *Geophysical Research Letters* 20, 1483–1486.
- Singh, S.K., Suárez, G., Domínguez, T., 1985. The great Oaxaca earthquake of January 1931: lithosphere normal faulting in the subducted Cocos plate. *Nature* 317, 56–58.
- Timoshenko, S., Goodier, J.N., 1951. *Theory of Elasticity*, 2nd ed. McGraw-Hill Book Co., New York.
- Tovish, A., Schubert, G., Luyendyk, B.P., 1978. Mantle flow pressure and the angle of subduction: non-Newtonian corner flows. *Journal of Geophysical Research* 83, 5892–5898.
- Turcotte, D.L., 1974. Are transform faults thermal contraction cracks? *Journal of Geophysical Research* 79, 2573–2577.
- Turcotte, D.L., Schubert, G., 2002. *Geodynamics*, 2nd ed. Cambridge University Press, New York.
- Valdes, C.M., Mooney, W.D., Singh, S.K., Lomnitz, C., Luetgert, J. H., Hellsley, C.E., Lewis, B.T.R., Mena, M., 1986. Crustal structure of Oaxaca, Mexico, from seismic refraction measurements. *Bulletin of the Seismological Society of America* 76, 547–563.
- van Hunen, J., van den Berg, A., Vlaar, N., 2002. On the role of subducting oceanic plateaus in the development of shallow flat subduction. *Tectonophysics* 352, 317–333.
- van Keken, P.E., Kiefer, B., Peacock, S.M., 2002. High resolution models 716 of subduction zones: implications for mineral dehydration reactions and the transport of water into deep mantle. *G-cubed* 3 (10), 20.
- Watts, A.B., 2001. *Isostasy and flexure of the lithosphere*. Cambridge University Print, Cambridge, New York. 458 pp.
- Zhu, A., Wiens, D., 1991. Thermoelastic stress in oceanic lithosphere due to hotspot reheating. *Journal of Geophysical Research* 96 (B11), 18323–18334.